Synthesis, structure and electrical conductivity of a new perovskite type barium cobaltate BaCoO1.80(OH)0.86

Waidha, Aamir; Lepple, Maren ; Benes, Alexander ; Wissel, Kerstin ; Fortes, A.D. ; Wollstadt, Stephan ; Slater, Peter; Clemens, Oliver

DOI:
10.1039/C8DT01326H

Document Version
Peer reviewed version

Synthesis, structure and electrical conductivity of a new perovskite type barium cobaltate BaCoO1.80(OH)0.86

Clemens, Oliver; Slater, Peter; Waidha, Aamir; Lepple, Maren ; Wissel, Kerstin ; Benes, Alexander ; Wollstadt, Stephan ; Fortes, A.D.

DOI:
DOI: 10.1039/C8DT01326H

Dalton Transactions

Accepted Manuscript

This article can be cited before page numbers have been issued, to do this please use: A. I. Waidha, M. Lepple, A. Benes, K. Wissel, A. D. Fortes, S. Wollstadt, P. Slater and O. Clemens, *Dalton Trans.*, 2018, DOI: 10.1039/C8DT01326H.

ROYAL SOCIETY OF CHEMISTRY

rsc.li/dalton

View Article Online
DOI: 10.1039/C8DT01326H

Synthesis, structure and electrical conductivity of a new perovskite type barium cobaltate $BaCoO_{1.80}(OH)_{0.86}$

Aamir Iqbal Waidha[a], Maren Lepple[b], Kerstin Wissel[a], Alexander Benes[c], Stephan Wollstadt[a], Peter R. Slater[d], A.D. Fortes[e], Oliver Clemens[a,f*]

[a] Technische Universität Darmstadt, Institut für Materialwissenschaft, Fachgebiet Materialdesign durch Synthese, Alarich-Weiss-Straße 2, 64287 Darmstadt, Germany.

[b] Technische Universität Darmstadt, Eduard-Zintl-Institut für Anorganische und Physikalische Chemie, Alarich-Weiss-Straße 12, 64287 Darmstadt, Germany.

[c] Technische Universität Darmstadt, Institut für Materialwissenschaft, Fachgebiet Gemeinschaftslabor Nanomaterialien, Alarich-Weiss-Straße 2, 64287 Darmstadt, Germany.

[d] University of Birmingham, School of Chemistry, Edgbaston, Birmingham B15 2TT, UK

[e] ISIS Facility, Rutherford Appleton Laboratory, Harwell Science and Innovation Campus, Didcot, Oxfordshire OX11 0QX, United Kingdom

[f] Karlsruher Institut für Technologie, Institut für Nanotechnologie, Hermann-von-Helmholtz-Platz 1, 76344 Eggenstein Leopoldshafen, Germany.

* Corresponding Author:

Fax: +49 6151 16 21991

E-Mail: oliver.clemens@md.tu-darmstadt.de

View Article Online
DOI: 10.1039/C8DT01326H

Abstract

Perovskite oxides exhibiting mixed protonic and electronic conductivities have interesting applications in protonic ceramic fuel cells. In this work, we report on a hydrated phase of $BaCoO_{1.80}(OH)_{0.86}$ synthesized using nebulized spray pyrolysis. Structural analysis based on X-ray and neutron powder diffraction data showed that the compound is isotypic to $BaFeO_{2.33}(OH)_{0.33}$. The water loss behaviour was studied using simultaneous thermal analysis and high temperature X-ray diffraction, indicating that protons (respectively water) can be stabilized within the compound up to temperatures significantly above 673 K, confirmed by ex-situ Fourier transform infrared spectroscopy studies. Impedance spectroscopy was used to determine the conductivity characteristics of $BaCoO_{1.80}(OH)_{0.86}$, finding and a total electrical conductivity in the order of 10^{-4} S cm^{-1} at ambient temperature with an activation energy of 0.28 eV.

Keywords

Perovskites; PCFC; electrode catalysts; neutron diffraction; impedance spectroscopy

View Article Online
DOI: 10.1039/C8DT01326H

1 Introduction

Perovskite type compounds ABX_3 (A = alkaline earth or lanthanide, B = transition metal, X = anion, e. g. oxide, fluoride, hydroxide) have attracted a lot of attention over the past years due to their interesting electronic, magnetic and optical properties [1, 2]. The structure of the cubic aristotype (space group *Pm*-3*m*) can be understood as being built up by a cubic close packed arrangement of AX_3 layers with the B cations occupying 1/4th of the octahedral voids. This arrangement is highly flexible with respect to the formation of large amounts of anion vacancies, with values of y up to 1 in $ABX_{3-y}\square_y$ being possible[3,4]. Those anion vacancies can be filled with a variety of anion species by the use of topochemical reactions [5,6]. For Ba-rich compounds, it is known that the anion vacancies can be filled with large amounts of water, resulting in proton-conducting compounds [7,8]. Such compounds are of high interest for the use in proton conducting solid oxide fuel and electrolysis cells (SOFC / SOEC, also often referred to as protonic ceramic fuel cells PCFCs). A prominent example is Y-doped $BaZrO_3$, which is a promising candidate as an electrolyte material due to its high proton and negligible electronic conductivity [8,9]. In contrast, only few compounds are known to be suitable as electrode catalysts for the oxygen side of PCFCs, which require the use of first row transition metal species (e. g. Mn, Ni, Co, Mn, Fe) to show sufficient electronic conductivity and therefore catalytic activity. In an aim to investigate water uptake and proton conductivity of such systems, our group recently reported the first studies on the water uptake and proton conductivity of $BaFeO_{2.5}$ [10-12]. In these studies, we found that monoclinic $BaFeO_{2.5}$ can take up relatively large amounts of water to form compounds with composition $BaFeO_{2.33}(OH)_{0.33}$ (LW-$BaFeO_{2.5}$, LW = low water) and $BaFeO_{2.25}(OH)_{0.5}$ (HW-$BaFeO_{2.5}$, HW = high water) accompanied by an increase of conductivity due to incorporation of the protons [10].

Cobaltates with perovskite type structure (such as $La_{1-x}Sr_xFe_{1-y}Co_yO_{3-d}$ [13] and $Ba_{0.5}Sr_{0.5}Co_{0.8}Fe_{0.2}O_{3-d}$ [14]) are known for their excellent catalytic properties as oxygen electrode catalysts [13,15]. Regardless of this, no studies have been reported on the proton uptake of barium cobaltates $BaCoO_{3-y}$ with cubic close packed BaO_{3-y} lattice. The lack of such studies might relate to the difficulty of stabilizing barium cobaltates in *ccp* related perovskite type structure, with $BaCoO_{2.22}$ [6] and trigonal $BaCoO_2$ [16] being the only known

View Article Online
DOI: 10.1039/C8DT01326H

two compounds which adopt this structural arrangement. Compounds with higher oxygen content were found to crystallize in various hexagonal perovskite type structures: 5H-$BaCoO_{2.8}$ [17], 12H-$BaCoO_{2.61}$, [18], 2H-$BaCoO_3$ [19, 20,21,22], Mn-doped 10H-$BaCoO_3$ [23].

In this article we report on the preparation of a new hydrated barium cobaltate phase with approximate composition $BaCoO_{1.80}(OH)_{0.86}$, which is found to be isotypic to LW-$BaFeO_{2.5}$ ($BaFeO_{2.33}(OH)_{0.33}$) [10] from a structural analysis on a deuterated sample via Rietveld refinement of X-ray and neutron powder diffraction (XRD, NPD). High temperature XRD (HT-XRD), Fourier transform infrared spectroscopy (FTIR) and simultaneous thermal analysis (STA) were used to study the stability range of this phase with respect to water loss. Additionally, electrochemical impedance spectroscopy (EIS) was used to investigate the electrical conductivity of the new material.

2 Experiment

2.1 Material synthesis

$BaCoO_{1.80}(OH)_{0.86}$ was synthesized using nebulized spray pyrolysis (NSP). To prepare the starting precursor solution, $Ba(NO_3)_2$ (Sigma Aldrich,99.99%) and $Co(NO_3)_2{\cdot}6H_2O$ (Sigma Aldrich,99.99%) were dissolved in de-ionized water at a cation concentration of 0.06 mol l^{-1}, and the mixture was stirred for 30 minutes in order to obtain a homogenous pinkish transparent solution. For the synthesis, a setup as previously described in [24] was used. The as-prepared solution was injected into the nebulizer unit using a syringe pump with the flow rate of 1.5 ml min^{-1}, while operating the ultrasonicator required to generate the mist at a generator voltage and current of 47.0 V and 0.51 A respectively. The precursor mist formed inside the nebulizer unit was transported by a carrier gas stream of argon at the rate of 2 SLM (standard liter per minute) to the reaction tube, which was maintained at 1323 K. The as-synthesized particles were collected on glass filter paper in the collector unit. The collector unit was maintained at 373 K to prevent water vapor condensation. The whole process was carried out at the constant pressure of 900 mbar.

For electrical characterization, pellets of the title compound were prepared by uniaxially pressing the powder followed by a subsequent isostatic pressing at a pressure of 700 kN. Pellets were then sputtered with a thin layer of gold on both sides for electronic contacting.

View Article Online
DOI: 10.1039/C8DT01326H

2.2 Diffraction experiments

XRD patterns of the hydrated compound were recorded on a Bruker D8 diffractometer using Bragg-Brentano geometry with a fine focusing X-ray tube with Cu $K_{\alpha 1,2}$ radiation. A VANTEC detector (3° opening) and a variable divergence slit (4 mm) were used. The total scan time was set to 10 hours for the angular range between 5° and 130° 2θ at a step size of 0.0075°. High temperature XRD was measured using an Anton Paar HTK1200 sample stage in the temperature range between 303 K and 1023 K (heating rate of 5 K s^{-1}) in the angular range between 20° and 60° 2θ with the step size of 0.0075° (total counting time of 10 min per scan) under a flow of argon. These conditions were chosen as a compromise to obtain sufficient data quality for the determination of lattice parameters and phase composition, but to lower differences to the heating procedure used for simultaneous thermal analysis.

Time-of-flight (TOF) neutron powder diffraction (NPD) data were recorded on the high resolution diffractometer (HRPD) at the ISIS pulsed spallation source (Rutherford Appleton Laboratory, Didcot, U.K.).2 g of powdered $BaCoO_{1.80}(OH)_{0.86}$ was loaded into 8-mm-diameter thin-walled cylindrical vanadium sample cans, and data were collected at ambient temperature for a 314 μAh proton beam current to the ISIS target corresponding to the beam time of ~7.5 h.

The analysis of the nuclear structure of $BaCoO_{1.80}(OH)_{0.86}$ using both the NPD and XRD data was performed using the Rietveld method with the program TOPAS 5 (Bruker AXS, Karlsruhe, Germany) [25]. For the room temperature XRD data, the whole 2θ-range range was used, while for NPD, data collected from the high resolution backscattering detector bank (bank 1) as well as the 90° high intensity bank (bank 2) were used. The instrumental intensity distribution for the X-ray data was determined empirically from a sort of fundamental parameters set [26], using a reference scan of LaB_6 (NIST 660a), and the microstructural parameters were refined to adjust the peak shapes for the XRD data. The lattice parameters were constrained to be the same for neutron and XRD data, and the same positional parameters were used and refined for both data sets. Independent thermal displacement parameters were refined for each type of atom for neutron data. As a starting model, our structural model of LW-$BaFeO_{2.33}(OH)_{0.33}$ as described in [10] was used.

View Article Online
DOI: 10.1039/C8DT01326H

2.3 Simultaneous thermal analysis and elemental analysis

Simultaneous thermal analysis combining thermogravimetric analysis (TGA) and differential scanning calorimetry (DSC) was conducted for $BaCoO_{1.80}(OH)_{0.86}$ on a Netzsch STA 449 F3 Jupiter thermal analyzer. The measurements were performed in the temperature range between 300 K to 973 K using a heating rate of 10 K min^{-1}. Thermal analysis was performed in corundum crucibles under an argon flow of 50 ml min^{-1}.

Elemental analysis was performed on a VarioEL III CHN (Elementar). The samples were burned in Sn boats under oxygen, and the evolving gases were gas chromatographically separated and analyzed quantitatively with a thermal conductivity detector. The hydride content was determined as the mean of four measurements.

2.4 Fourier-transform infrared spectroscopy

Fourier-transform infrared spectroscopy measurements were conducted on a Varian spectrometer. Samples were characterized via attenuated total reflection (ATR) by mounting an ATR unit into the sample compartment of the spectrometer. The spectra were recorded in a range between 550 cm^{-1} and 4000 cm^{-1} with a spectral resolution of 0.5 cm^{-1}.

2.5 X-ray photoelectron spectroscopy

The surface composition and oxidation states were examined by ex-situ X-ray photoelectron spectroscopy (XPS) analysis using a Physical Electronic VersaProbe XPS unit (PHI 5000 spectrometer) with Al K_α radiation (1486.6 eV). All detail spectra were recorded with 50.6 W, a step size of 0.1 eV and a pass energy of 23.5 eV. The binding energies were calibrated with respect to the carbon 1s (C1s) emission line at 284.8 eV.

2.6 Impedance spectroscopical analysis

Alternating current electrochemical impedance spectroscopy measurements were carried out to record the conductivity of the $BaCoO_{1.80}(OH)_{0.86}$ pellet. The pellet was placed inside the JANIS STVP-200-XG cryostat, which was operated under static helium atmosphere of 1 bar pressure. The pellet was investigated in the temperature range of 228 K to 298 K. Impedance measurements were recorded using a Solartron 1260 frequency response analyzer while applying an AC signal of 100 mV amplitude with

View Article Online
DOI: 10.1039/C8DT01326H

frequency ranging from 1 MHz to 100 mHz. Fitting of the data was performed using the Z-view program [27].

2.7 Scanning Electron Microscopy and Energy Dispersive X-ray Spectroscopy

The scanning electron microscopy (SEM) images were taken using the secondary electron detector of a Philips XL30 FEG scanning electron microscope operating at 30 keV. For energy dispersive spectroscopy (EDAX) analysis the EDAX Genesis system was used and an energy resolution of about 140 eV was applied. The mapped area was of the order of 100 μm² and the Ba to Co ratio was determined from the Ba L and Co K lines. The sample was sputtered with approximately 10 nm of Au prior to the measurements. The mean particle diameter was determined using the software "image j".

3 Results and discussion

3.1 Microstructure, composition and crystal structure of $BaCoO_{1.80}(OH)_{0.86}$

The morphology of the as-synthesized powder was studied with scanning electron microscopy (SEM, see Figure 1). The formation of spherical hollow particles could be observed, with particles showing a mean diameter of 0.3 μm, which is a typical morphology obtained with this method according to our experience [24, 28].

Elemental analysis of the powder was carried out using energy dispersive X-ray spectroscopy (EDAX, see Figure S1 in the SI), which confirmed a 1:1 ratio of Ba:Co (experimentally 1:1.02(2)). The average oxidation state of Co was determined by iodometric titration and found to be $Co^{+2.46(2)}$, corresponding to an approximate composition of $BaCoO_{2.22-x}(OH)_{2x}$. This oxidation state is similar to what has been found by Mentré et al. for their highly oxygen deficient phase $BaCoO_{2.22}$ [6]. We found that the compound contained significant amount of water, and the content of crystalline water could be approximated to 0.43 H_2O per formula unit (see high temperature behavior of the compound reported in section 3.2). From the analyses performed, we conclude that the compound has an approximate overall composition of $BaCoO_{2.22}(H_2O)_{0.43}$ = $BaCoO_{2.66}H_{0.86}$ = $BaCoO_{1.80}(OH)_{0.86}$. This water content was further verified by elemental

View Article Online
DOI: 10.1039/C8DT01326H

hydrogen analysis (0.43(2) wt-% of H in comparison to a theoretical weight fraction of H of 0.37 wt-%).

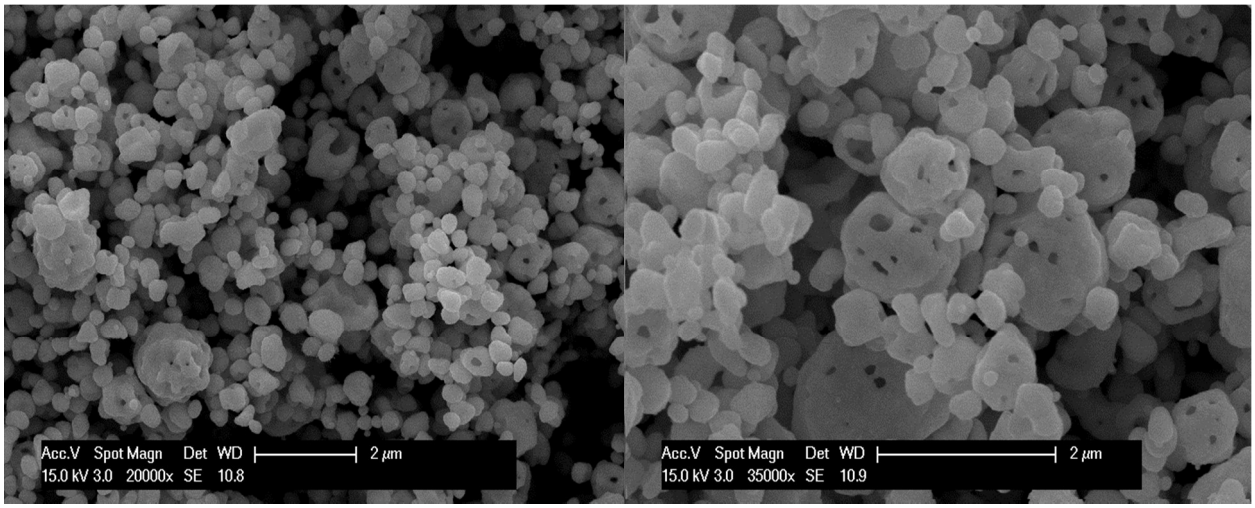

Figure 1: SEM micrographs of as-synthesized $BaCoO_{1.80}(OH)_{0.86}$ powder.

For structural analysis, the compound was prepared using deuterium oxide as the solvent, and examined via X-ray and neutron powder diffraction. $BaCoO_{1.80}(OD)_{0.86}$ showed diffraction patterns (see Figure 2) with reflection groups significant for the presence of a distorted perovskite type phase with *ccp* stacking of the BaX_y layers. The patterns showed a clear resemblance to the ones of LW-$BaFeO_{2.33}(OH)_{0.33}$, which is a 6 x $2\sqrt{2}$ x $\sqrt{2}$ superstructure of the cubic aristotype structure (space group *Cmcm*) and was reported previously by our group [10]. Pawley Fits were used to confirm the validity of this symmetry. For LW-$BaFeO_{2.33}(OH)_{0.33}$ [10] the symmetry lowering originates from an ordering of anion vacancies in the anion deficient lattice. The observation of structural similarity for both compounds is chemically plausible, since $BaCoO_{1.80}(OD)_{0.86}$ has a (nearly) identical overall content of anion vacancies. Therefore, the structure of $BaCoO_{1.80}(OD)_{0.86}$ was refined using the structural model of LW-$BaFeO_{2.33}(OH)_{0.33}$ [10] as the starting model.

It was previously shown by V. Jayaraman et. al. that deuterated samples can facilitate the identification of the deuterium positions within a perovskite lattice [29]. In the case of $BaCoO_{1.86}(OD)_{0.86}$, coupled analysis of XRD and NPD data gives the potential to have high scattering contrasts between the different types of atoms, since strong X-ray scatterers (Ba and Co) are present next to weak X-ray scatterers (O), and strong

View Article Online
DOI: 10.1039/C8DT01326H

neutron scatterers (Ba, O and D) are present next to weak nuclear scatterers (Co). We attempted to identify potential D positions by Fourier difference mapping, which were then used as starting positions for the structural analysis. Although scattering contrasts are good, we observed strong correlations between structural parameters when using a very flexible refinement model (e. g., with independent thermal parameters for all oxygen ions, refining site occupancies for oxygen, or when using anisotropic thermal parameters), therefore, chemically plausible constraints were used (e. g., identical thermal parameters for same types of atoms, fixing of oxygen occupancies). For the location of deuterium, a very strong correlation with the occupancy factor was observed, which we took into account by limiting the thermal parameter to a value of 5 Å² (both parameters increased when refining independently). The refined deuterium content accounts for 0.77 of the 0.86 D atoms present in the compound; therefore, parts of the D atoms could not be located. Bond valence sums [30] give some indication that the O3 and O4 require some further cations in their coordination sphere, however, localization of further D atoms close to these ions did not prove to be successful.

By this, we obtained a good fit to the pattern (Figure 2) based on a chemically plausible structural model (see Table 1), with bond distances given in Table 2. The D-O bond lengths are in the order of 1.3 - 1.4 Å. This value is too high for a deuterium ion being strongly localized within a covalent D-O bond, which we think could relate to a poor localization of the deuterium between the two neighbouring oxide ions.

Water incorporation into anion deficient perovskites has been reported [31] to occur based dissociation and on the formation of hydroxide groups according to

$$H_2O + V_O^{\bullet\bullet} + O_O \rightarrow 2\,(OH)_O^{\bullet}$$

Alternatively, one could imagine water to be incorporated in a molecular manner according to

$$H_2O + V_O^{\bullet\bullet} \rightarrow (OH_2)_O^{\bullet\bullet}$$

The high concentration of 1.5 D1 atoms around O7 could therefore indicate a partial occupation as crystalline water; however, the difficulties in exactly localizing and quantifying the D atoms within the refinement shows that this should not be overinterpreted.

View Article Online
DOI: 10.1039/C8DT01326H

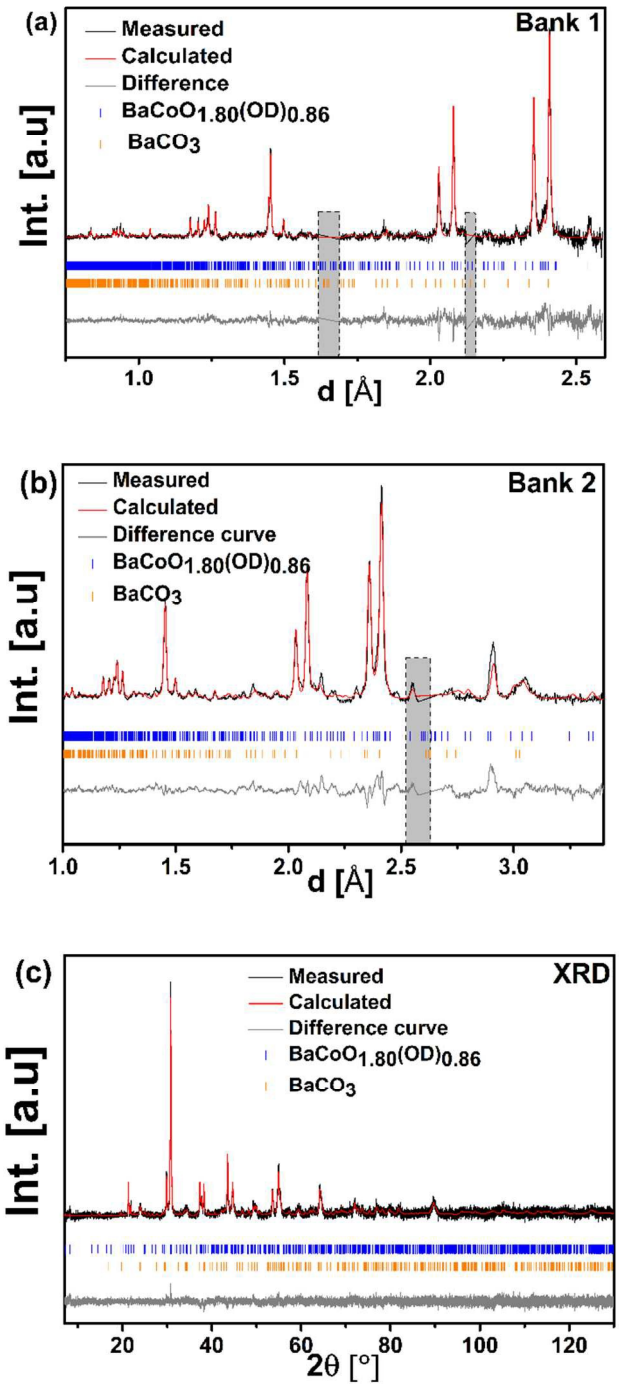

Figure 2: Coupled Rietveld analysis of neutron and X-ray powder diffraction patterns of $BaCoO_{1.80}(OD)_{0.86}$. Reflection groups (marked with grey boxes) with strong intensity contributions of $BaCO_3$ (identified by a different shape) were omitted from the neutron diffraction data due to unfavourable correlation with the structural parameters of the main phase.

View Article Online
DOI: 10.1039/C8DT01326H

Table 1. Structural parameters for refined $BaCoO_{1.80}(OD)_{0.86}$ presented along with the unit cell parameters, GOF and R_{wp} values. Standard deviations given are numerical standard deviations from the refinement and do not necessarily represent an interval of trust. The refined composition is $BaCoO_{1.80}(OD)_{0.77}$ due to the fact that the thermal parameter had to be fixed to take into account the strong correlation with site occupancies.

Label	**Atom**	**site**	**x**	**y**	**Z**	**Occ**	**Beq.**
Ba1	Ba^{2+}	4*c*	**0**	0.6030(8)	¼	1	1.27(4)
Ba2	Ba^{2+}	4*c*	**0**	0.16118(8)	¼	1	
Ba3	Ba^{2+}	8*g*	0.8292(3)	0.1371(6)	¼	1	
Ba4	Ba^{2+}	8*g*	0.3417(3)	0.1317(6)	¼	1	
Co1	$Co^{2.46+}$	8*g*	0.7519(6)	0.3956(12)	¼	1	0.80(3)
Co2	$Co^{2.46+}$	8*g*	0.5713(5)	0.3364(10)	¼	1	
Co3	$Co^{2.46+}$	8*g*	0.0779(6)	0.3764(13)	¼	1	
O1	O^{2-}	4*c*	**0**	0.8620(14)	¼	1	2.24(2)
O2	O^{2-}	4*c*	**0**	0.3808(15)	¼	1	
O3	O^{2-}	8*g*	0.7429(4)	½	¼	1	
O4	O^{2-}	8*g*	0.3343(5)	0.3751(11)	¼	1	
O5	O^{2-}	8*d*	$^1/_4$	$^1/_4$	**0**	1	
O6	O^{2-}	8*e*	0.4147(6)	**0**	**0**	1	
O7	O^{2-}	8*e*	0.9247(4)	**0**	**0**	1	
O8	O^{2-}	16*h*	0.0809(5)	0.2601(6)	0.9887(14)	1	
D1	D^+	16*h*	0.2740(3)	0.2629(9)	0.293(3)	0.75(2)	5
D2	D^+	16*h*	0.5507(8)	0.5443(11)	0.700(5)	0.40(2)	
***a* [Å]**	24.2965(8)	***b* [Å]**	11.9436(4)	***c* [Å]**	5.7693(2)		
GOF [XRD+NPD]		1.38		***R_{wp}* [%] [XRD+NPD]**		2.55	
R_{Bragg} [%]	1.14 **[XRD]**		3.95 **[NPD bank 1]**				

View Article Online
DOI: 10.1039/C8DT01326H

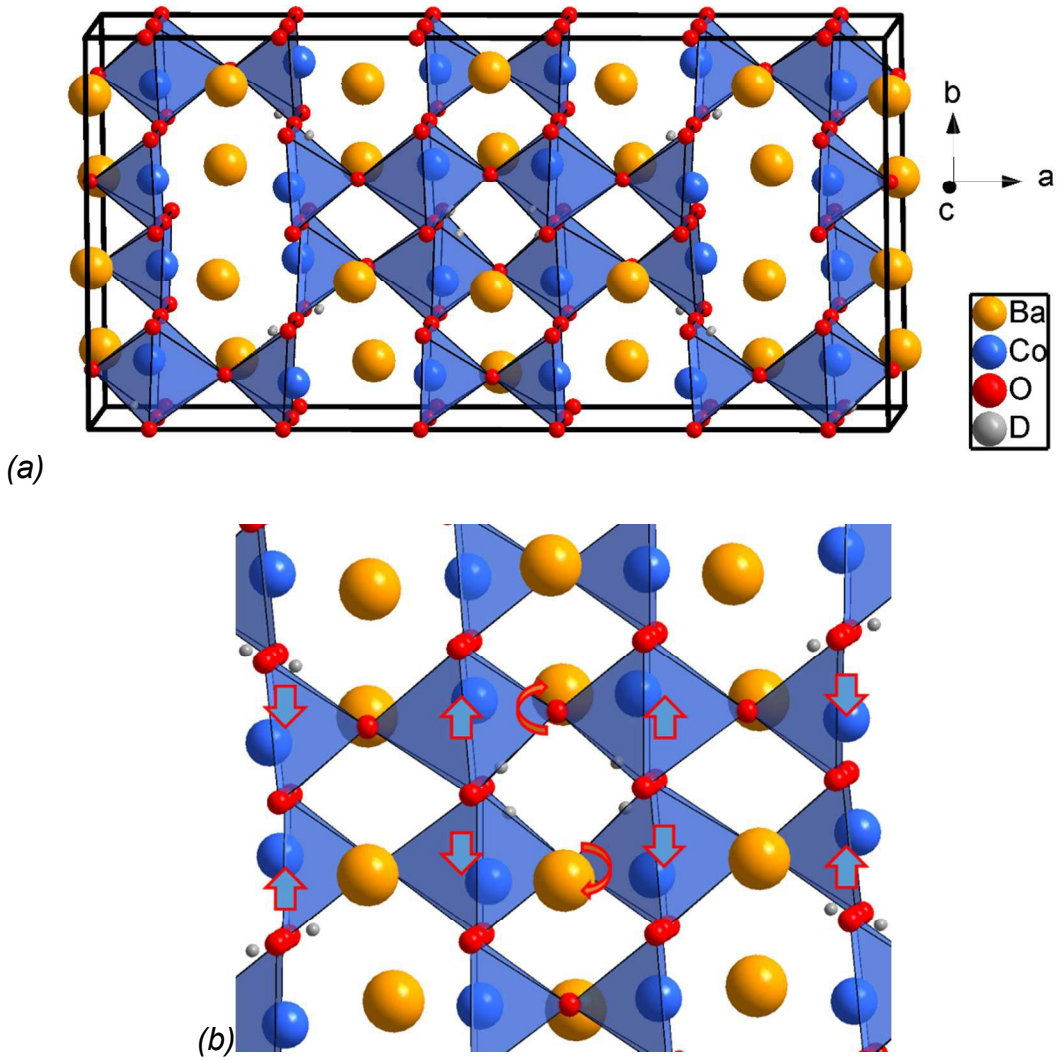

Figure 3: (a) Structural representation of $BaCoO_{1.80}(OD)_{0.86}$. (b) Excpanded diagram with an indication of cation relaxation around protonated oxygen ions.

A schematic of the structure is provided in Figure 3. It is found that strong structural relaxations occur in order to account for the incorporation of a large amount of protons. The Co ions appear to shift away from the oxide ions, which are close to the determined deuterium positions within the structure. In addition, the Ba ions shift strongly around the OD groups, whereas they reside closer to their ideal position when no deuterium is close. This need for structural relaxations on water incorporation is also well expressed by the change of cell volume on water uptake. Hydrated phases of Ba-rich perovskites with high water content $BaMO_y(OH)_z$, such as $BaInO_2OH$ [32,33], $BaFeO_{2.33}(OH)_{0.33}$ [10], and $BaFeO_{2.25}(OH)_{0.5}$ [10] are known for having a significantly higher volume per $BaMX_{y+z}$ unit (X = O, OH) than their water free counterparts $BaMO_{y-0.5z}$. Such differences in the

View Article Online
DOI: 10.1039/C8DT01326H

volumes per formula unit can be easily visualized from the calculation of a pseudocubic lattice parameter ($a_{ps.cub}$ = $(V_{f.u.})^{1/3}$) from the cube root of the volume per $BaCoX_{3-y}$ formula unit ($V_{f.u.}$). In agreement with the presence of water in the compound, the pseudocubic lattice parameter of $BaCoO_{1.80}(OH)_{0.86}$ (4.12 Å) was found to be significantly higher than the one of $BaCoO_{2.22}$ (4.08 Å [6, 11, 12], which can be considered as the corresponding water-free oxide). This volume difference is further similar to what was observed for the transformation of $BaFeO_{2.33}(OH)_{0.33}$ (4.14 Å) to $BaFeO_{2.5}$ (4.078 Å) [10].

The mixed valency of Co as determined from iodometric titration further agrees with the calculation of bond valence sums [30], which indicate an overall oxidation state of +2 for Co1 / Co3 and a significantly increased oxidation state of +2.49 for Co2.

Table 2: Refined bond distances between cations and anions for $BaCoO_{1.80}(OD)_{0.86}$.

Cation	Distances to anions [Å]	Cation	Distances to anions [Å]	Cation	Distances to anions [Å]
Ba1	2.65 (2) (O2 x 1)	Ba3	2.76(2) (O5 x 2)	Co1	1.92(1) (O3 x 2)
	2.80 (2) (O6 x 4)		2.80(1) (O3 x 2)		2.11(2) (O4 x 1)
	2.89 (1) (O2 x 2)		2.89(1) (O4 x 2)		2.26(1) (O5 x 2)
	2.90 (1) (O8 x 4)		3.03(1) (O8 x 2)		
			3.13(2) (O4 x 1)		
			3.19(1) (O7 x 1)		
Ba2	2.62 (2) (O2 x 1)	Ba4	2.67(1) (O8 x 2)	Co2	1.76(1) (O1 x 1)
	2.75 (1) (O8 x 4)		2.78(1) (O6 x 2)		1.81(1) (O8 x 2)
	2.90 (2) (O1 x 2)		2.91(2) (O4 x 1)		2.34(2) (O4 x 1)
	3.02 (2) (O7 x 4)		3.01 (1) (O5 x 2)		2.43(1) (O7 x 2)
			3.21(1) (O3 x 2)		
				Co3	1.89(1) (O2 x 1)
					2.05(1) (O8 x 2)
					2.07(1) (O6 x 2)

3.2 Temperature stability of $BaCoO_{1.80}(OH)_{0.86}$

The presence of protons within the structure can be well monitored by ex-situ FT-IR studies recorded after heating the compound to various temperatures. Within those

View Article Online
DOI: 10.1039/C8DT01326H

measurements, a broad band was observed for $BaCoO_{1.80}(OH)_{0.86}$ at 298 K in the spectral range 3300-3500 cm^{-1}, which can be assigned to the OH stretching mode [10,34] (see Figure 4). Apart from FT-IR, the incorporation of OH groups is also reflected in distinct valence band features at 9.1 eV and 5.0 eV from XPS studies (see Figure S2 in the SI). Those features have also been observed previously at surfaces of materials with perovskite type structure[,35] as well as on other oxides [36].

FT-IR measurements were also carried out after heating as-synthesized powder of $BaCoO_{1.80}(OH)_{0.86}$ to various temperatures up to 1273 K under the flow of argon. In this respect, we found that the OH stretching mode disappeared when the compound was heated to temperatures above 673 K.

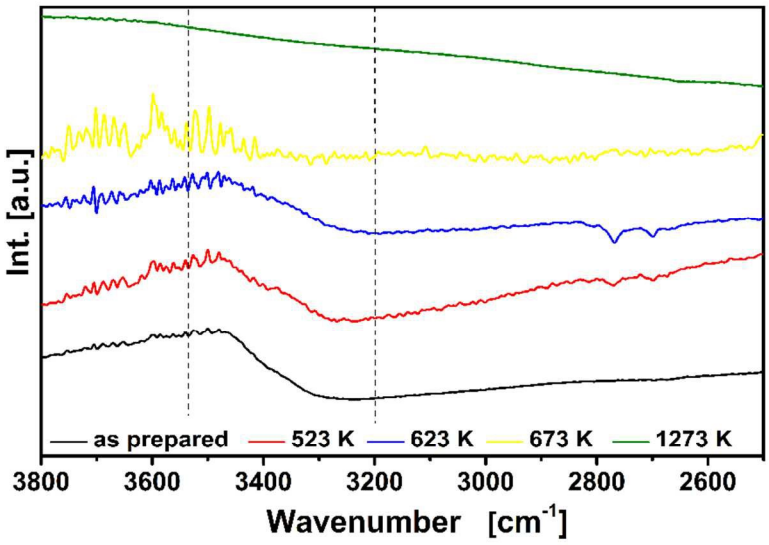

Figure 4: FTIR spectra for $BaCoO_{1.80}(OH)_{0.86}$ before and after heating to a variety of temperatures up to 1273 K.The curves are scaled to improve the visibility of the bump corresponding to the OH stretching band.

To study the water loss in more detail and to determine the amount of crystalline water, the sample was studied via simultaneous thermal analysis (STA, see Figure 5). TGA data show a steep weight loss between 398 K and 463 K accompanied with an endothermic signal. This indicates a first strong release of water, which is in agreement with the structural changes as found by high temperature XRD (see later in this section). After this first initial step, the weight loss continues until 750 K, at which the TGA shows

View Article Online
DOI: 10.1039/C8DT01326H

a clear kink. We therefore conclude, that the water release is finished between 693 - 793 K in this more dynamic experiment as compared to the FT-IR studies on heated powder. A total mass loss of ~ 2.8 - 3.2 wt-% was found, accounting for the presence of ~ 0.38 - 0.43 H_2O molecules per $BaCoX_{3-y}$ unit. From this and the average oxidation state of Co, one can determine the approximate composition of the sample to be $BaCoO_{2.22}(H_2O)_{0.43}$ = $BaCoO_{2.66}H_{0.86}$ = $BaCoO_{1.80}(OH)_{0.86}$.

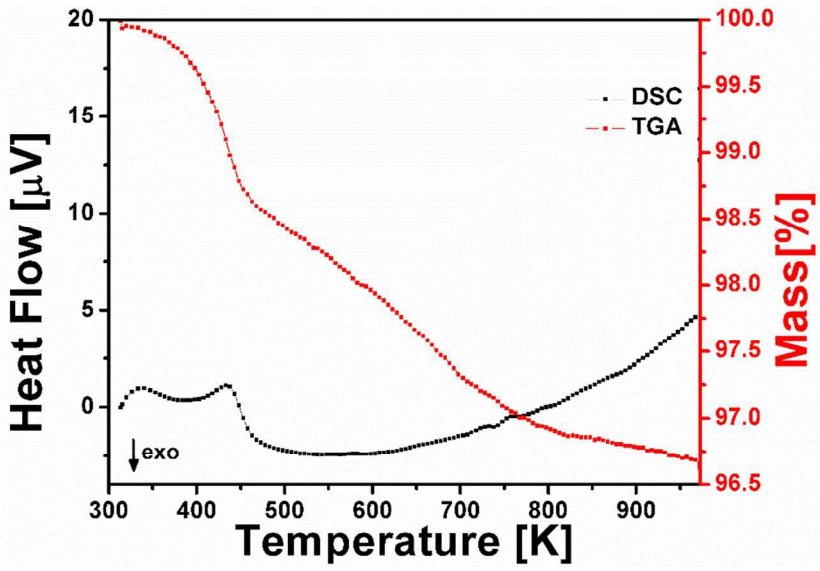

Figure 5: TGA/DSC measurement on $BaCoO_{1.80}(OH)_{0.86}$ under a flow of argon.

Changes on water loss were further studied by HT-XRD (see Figure 6). Although this methodology cannot provide detailed information on changes within the anion sublattice, it is well suited to investigate changes in phase fractions and unit cell volume on variation of temperature. For this analysis, the structural model of $BaCoO_{1.80}(OH)_{0.86}$ was used, without refining any positional parameters. Further, the reader needs to be aware that this study has different kinetics than the ex-situ FT-IR and in-situ STA measurements. Although a similar heating rate of 10°C min^{-1} was used for HT-XRD, the samples had to be kept at measurement temperature for at least 10 min to record a pattern of sufficient quality, i. e., from which lattice parameters and phase fractions could be determined. This need for longer holding times can shift the water losses to lower temperatures than what was observed for STA.

View Article Online
DOI: 10.1039/C8DT01326H

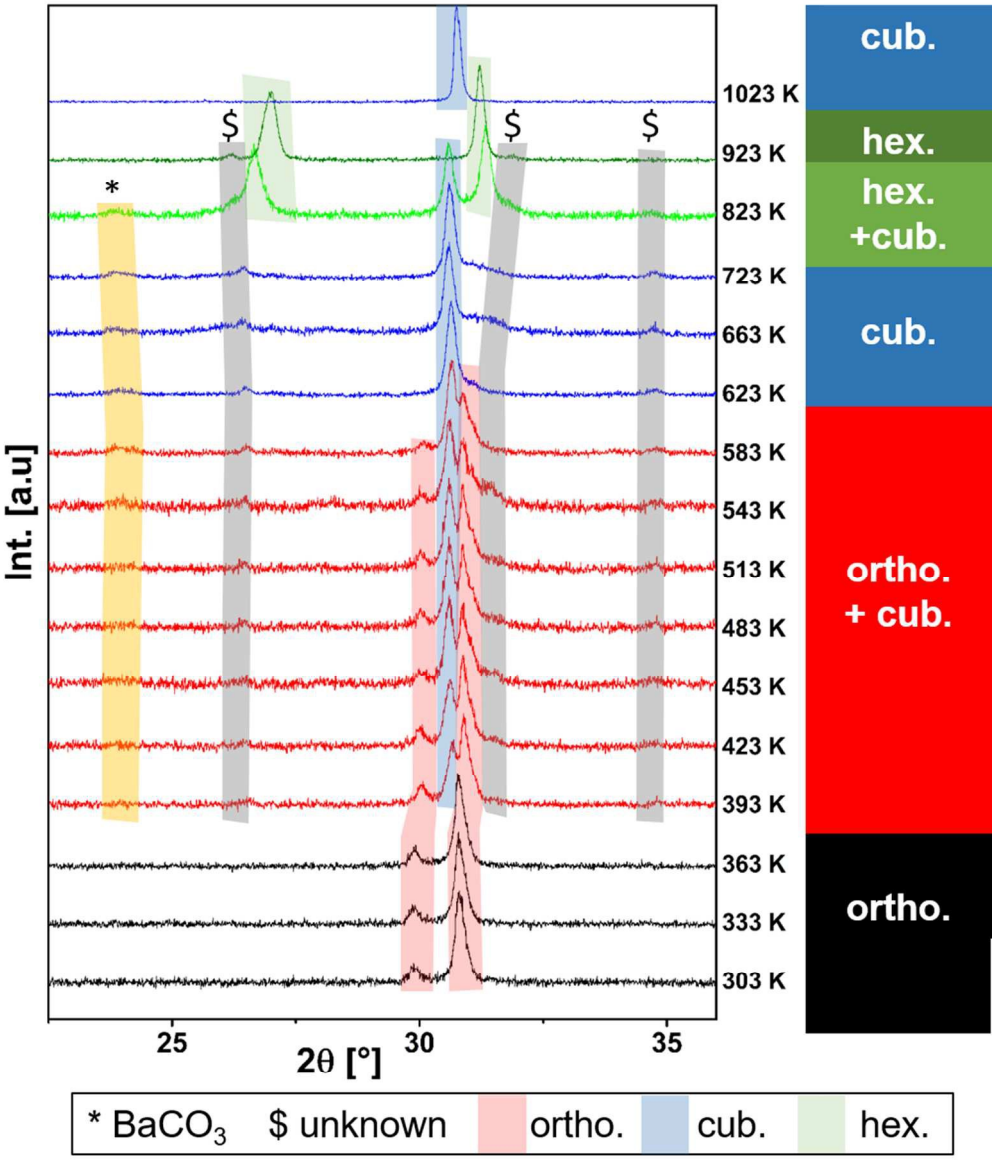

Figure 6: XRD patterns of $BaCoO_{1.80}(OH)_{0.86}$ recorded between 303 K and 1023 K under a flow of dry argon. Intensities are normalized to the reflection with maximum intensity.

Strong changes in the XRD pattern were observed above 393 K, which approximately coincides with the steep weight loss on first water release observed in STA. At this temperature, a second perovskite type phase with cubic symmetry (*Pm*-3*m*) can be detected, which coexists with the orthorhombic phase up to 583 K (see and Figure 7a) and becomes the main phase around 623 K (Figure 7b). The formation of a cubic phase on water loss could indicate that the chemical composition (i. e. the overall anion content) might be a strong driving force in order to stabilize the ordered orthorhombic structure of the water containing compound. In addition to the small amount of $BaCO_3$, a

View Article Online
DOI: 10.1039/C8DT01326H

small amount of a further reflections appeared at ~ 27°, 31° and 35° 2θ, which only disappear at the highest temperature of 1023 K. Attempts were made to index those reflections based on *klassengleiche* supergroups of the cubic (or orthorhombic) cell, which was not successful. The reflections were therefore assigned to an unknown impurity phase by ruling out known structures of $Ba_xCo_yO_z$ phases from the ICSD. The assignment to an impurity is also plausible considering that those reflections are still present at 923 K, where only a 2H hexagonal perovskite type phase was observed (see later in this section).

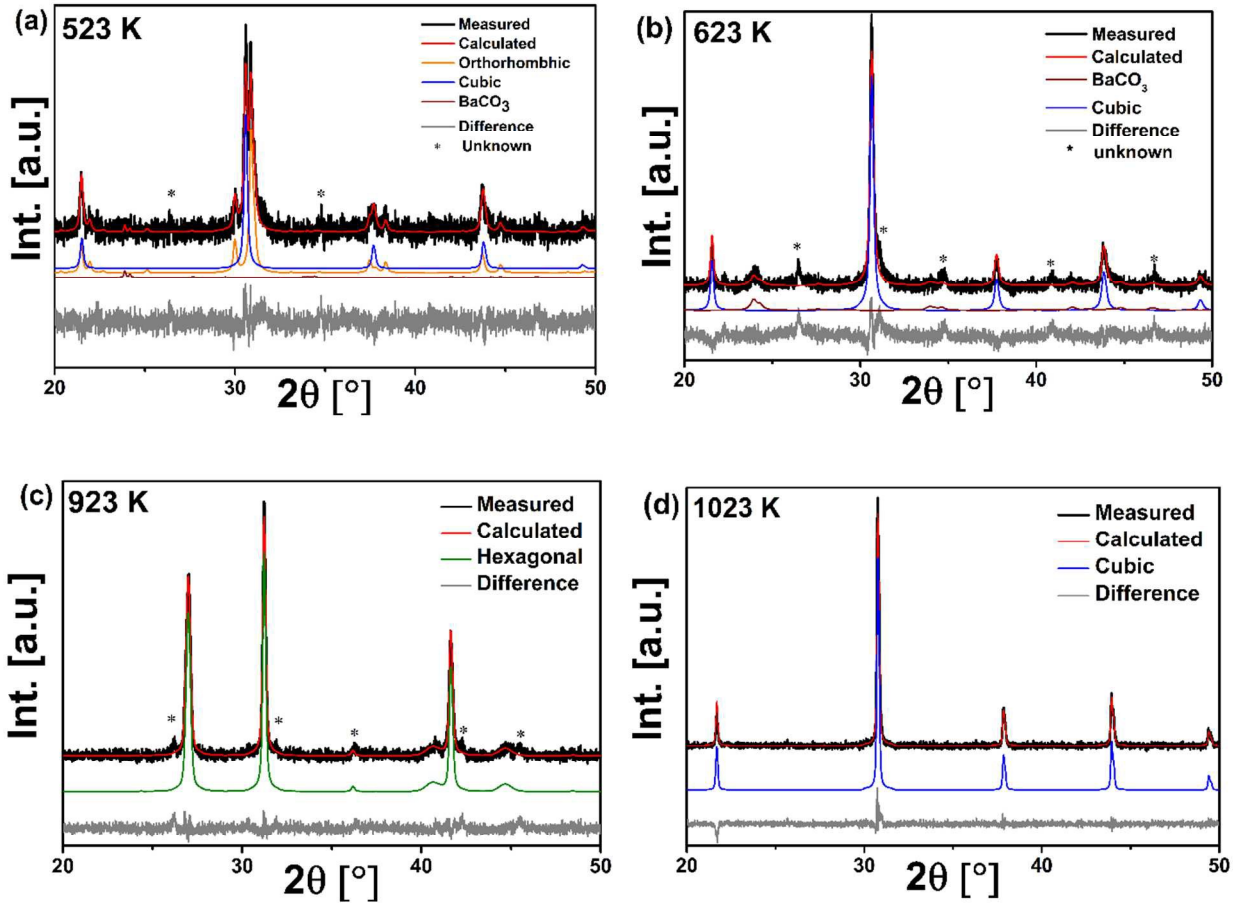

Figure 7: Rietveld analyses of high-temperature XRD data at representative temperatures. (a) Phase mixture of a cubic (*Pm*-3*m*) and orthorhombic (*Cmcm*) phase recorded at 523 K. (b) Cubic phase (*Pm*-3*m*) recorded at 623 K. (c) 2H perovskite type phase ($P6_3/mmc$) at 923 K. (d) Cubic phase (*Pm*-3*m*) recorded at 1023 K. Reflections of an unknown impurity phase are marked with an asterisk.

The water loss occurring at 393 K can be easily followed by the changes of the weight-fraction averaged pseudocubic lattice parameter $a_{ps.cub}$(average) (see Figure 8a), which

View Article Online
DOI: 10.1039/C8DT01326H

is a representative for the average cell volume per unit cell, and shows a sudden drop at this temperature. In addition, an anomaly of $a_{ps.cub.}$(orthorhombic) was observed. On water loss, the orthorhombic phase shows a decrease in cell volume (visually evident from the shifts of the reflections (see Figure 6)). Surprisingly, the newly formed cubic phase then has a higher value of $a_{ps.cub.}$ than the orthorhombic phase. The weight fraction of the cubic phase increases up to a temperature of 623 K, where it becomes the main perovskite type phase present up to 723 K (see Figure 7b and Figure 8b).

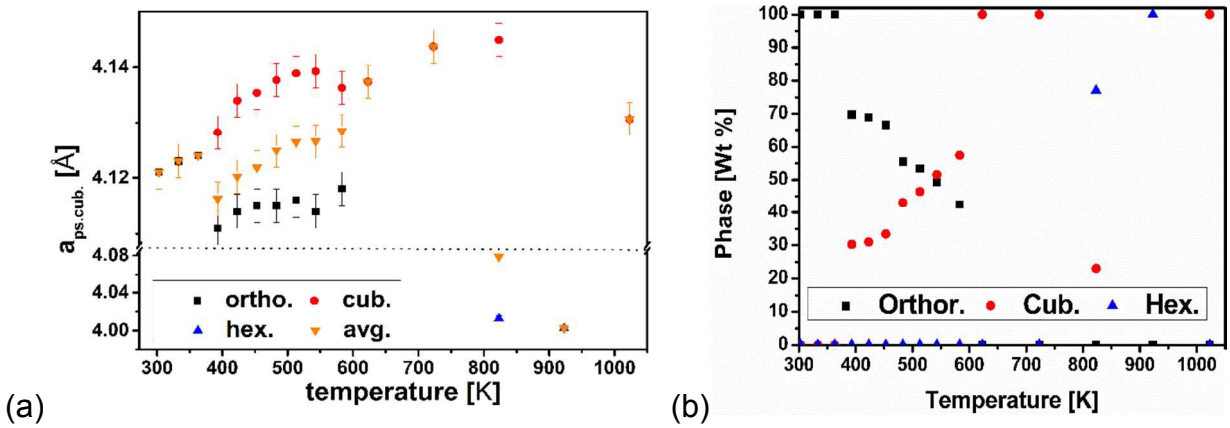

Figure 8: Pseudocubic lattice parameters (a) and relative phase fractions (b) of phases with perovskite type structure. Standard deviations are given as the numerical standard deviation of the refinement multiplied by 3. Numerical standard deviations obtained for the phase quantification do not represent a meaningful interval of trust, which is at least in the order of ~ 2 wt-% for such a phase quantification, and have therefore been omitted.

At a temperature of 623 K, the formation of an additional hexagonal perovskite type phase was observed (2H, $P6_3/mmc$, a = 5.7609(3) Å and c = 4.4613(4), see Figure 7c), which has a strongly reduced volume per formula unit as compared to the other phases (see Figure 8a). The relative fraction of this phase increases on heating to higher temperatures (see Figure 8b), and it becomes the only perovskite type phase at 923 K. Finally, a single phase cubic perovskite type compound is found at a temperature of 1023 K (see Figure 7d,a = 4.137 Å), similar to the reports on cubic $BaCoO_{2.22}$ by Mentré et al.[6].

Further, the observation of the cubic and hexagonal phases at high temperatures are similar to the findings described by Mentré et al. [6] in their high temperature study of $BaCoO_{2.22}$ (which can be considered as the water-free analogous composition to

View Article Online
DOI: 10.1039/C8DT01326H

$BaCoO_{1.80}(OH)_{0.86}$). They report [6] a transformation to a hexagonal compound at temperatures above ~523 K, and observed a retransformation to cubic on further heating. However, their temperature range of coexistence of cubic and hexagonal phases [6] is different than what was observed here on studying $BaCoO_{1.80}(OH)_{0.86}$, and this might indicate an influence of residual water on stabilization of the cubic symmetry.

We would like to point out that the observed changes in phases and cell volumes are different to what we found on heating HW-$BaFeO_{2.25}(OH)_{0.5}$ [10]. For this phase, we found a step-wise transformation to orthorhombic $BaFeO_{2.33}(OH)_{0.33}$ and monoclinic $BaFeO_{2.5}$, with narrow temperature ranges of co-existence of two phases. In future, we will aim to investigate the unusual phase changes for $BaCoO_{1.80}(OH)_{0.86}$ in more detail via a high temperature neutron diffraction study, for which data recorded at a diffractometer with higher neutron flux will be required.

3.3 Temperature dependent Conductivity studies

The conductivity of the title compound was studied by impedance spectroscopy in the temperature range between 298 K and 228 K. As for the ferrites [10], the preparation of sintered pellets of $BaCoO_{1.80}(OH)_{0.86}$ is not possible (explained by strong volume changes on water uptake of water-free sintered pellets, which result in the cracking of pellets); therefore, as-synthesized powder was compacted to stable pellets by means of isostatic pressing at a pressure of 700 kN, resulting in densities in the order of ~ 85 % relative to the crystallographic density.

Figure 9 shows an example of the NYQUIST and BODE plots of a typical impedance spectrum. The NYQUIST plot can be described as a strongly depressed semicircle, which can be well fitted by an equivalent circuit consisting of a resistance and a constant phase element (CPE) in parallel. In the low frequency range, the impedance is dominated by its real contribution, and no electrode response could be observed independent of the choice of the electrode material (sputter coated Au or Pt). This indicates a strong influence of electronic charge carriers and the compound behaves mainly like a simple resistor at frequencies below ~ 10 kHz. Relative permittivity of 80 – 150 indicate a predominance of grain and/or grain boundary phenomena on the overall conductivity [10].

View Article Online
DOI: 10.1039/C8DT01326H

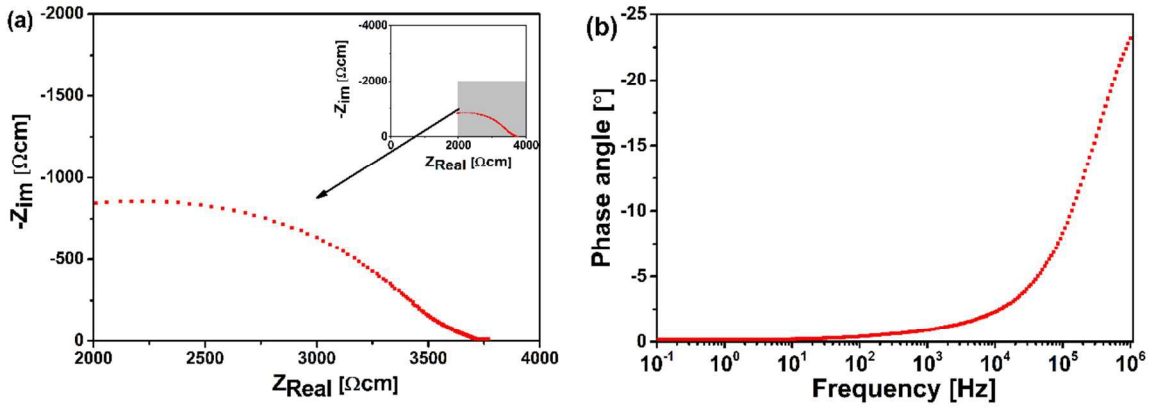

Figure 9: (a) NYQUIST and (b) BODE plots for the impedance spectroscopical measurement for $BaCoO_{1.80}(OH)_{0.86}$ recorded at 298 K.

The overall electrical conductivity of $BaCoO_{1.80}(OH)_{0.86}$ is in the order of ~10^{-4} S cm^{-1} at 298 K. This value is three orders of magnitude higher than what was observed for LW-$BaFeO_{2.5}$ and one order of magnitude higher than found for Y-doped $BaZrO_3$, most likely resulting from a different nature of the charge carrier. Therefore, we conclude that the electrical conductivity of $BaCoO_{1.80}(OH)_{0.86}$ is dominated by electronic charge carriers and that the determination of a protonic contribution to the overall conductivity is not easily possible. To separate those phenomena further techniques, e. g., quasi-elastic neutron scattering will be examined in the future. A high electronic conductivity is in agreement with cobalt being present in a mixed valent state, which can facilitate electronic charge transport via a hopping mechanism.

The temperature dependency of the conductivity is shown in Figure 10 for two different samples in the form of an Arrhenius type plot, from which the activation energy can be calculated to be 0.27(1) eV. Although small differences in total conductivity are found depending on the exact preparation, the overall magnitude of the conductivity can be well reproduced.

View Article Online
DOI: 10.1039/C8DT01326H

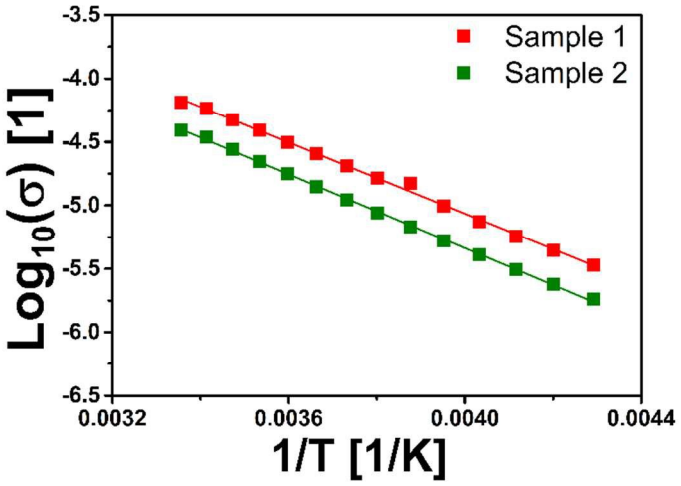

Figure 10: Arrhenius plot for temperature dependent total electrical conductivity of two samples of $BaCoO_{1.80}(OH)_{0.86}$ in the temperature range between 240 – 300 K.

4 Conclusions

Here we have shown that a new phase with approximate composition $BaCoO_{1.80}(OH)_{0.86}$ can be prepared by means of nebulized spray pyrolysis. The compound can be understood as the water rich analogue to $BaCoO_{2.22}$ [6], and was confirmed to be isotypic to LW-$BaFeO_{2.33}(OH)_{0.33}$ [10] by a coupled analysis of X-ray and neutron powder diffraction data. In comparison to $BaFeO_{2.5}$ [10], protons can be stabilized within this compound up to a much higher temperature of ~673 K, in agreement with findings by FT-IR, STA, and HT-XRD studies. Therefore, the results reported here indicate that Ba-rich $Ba(Co,Fe)O_{3-x}$ compounds could be interesting catalysts for the use in PCFCs. Furthermore, the material shows an unusual and complex structural behaviour on heating and water release, which will be investigated in more detail within future studies.

5 Acknowledgements

O. Clemens acknowledges funding by DFG within CL551/2-1. Neutron diffraction beamtime at ISIS was provided by the Science and Technology Facilities Council.

6 References

1. G. H. Jonker, *Journal of Applied Physics*, 1966, 37, 1424-1430.
2. M. L. Medarde, *J. Phys.: Condens. Matter*, 1997, 9.

View Article Online
DOI: 10.1039/C8DT01326H

3. C. Tassel, J. M. Pruneda, N. Hayashi, T. Watanabe, A. Kitada, Y. Tsujimoto, H. Kageyama, K. Yoshimura, M. Takano, M. Nishi, K. Ohoyama, M. Mizumaki, N. Kawamura, J. Iniguez and E. Canadell, *J Am Chem Soc*, 2009, 131, 221-229.
4. Y. Tsujimoto, C. Tassel, N. Hayashi, T. Watanabe, H. Kageyama, K. Yoshimura, M. Takano, M. Ceretti, C. Ritter and W. Paulus, *Nature*, 2007, 450, 1062-1065.
5. O. Clemens and P. R. Slater, *Reviews in Inorganic Chemistry*, 2013, 33, 105-117.
6. O. Mentre, M. Iorgulescu, M. Huve, H. Kabbour, N. Renaut, S. Daviero-Minaud, S. Colis and P. Roussel, *Dalton T*, 2015, 44, 10728-10737.
7. S. M. Haile, D. L. West and J. Campbell, *J Mater Res*, 1998, 13, 1576-1595.
8. Y. Yamazaki, R. Hernandez-Sanchez and S. M. Haile, *Chem Mater*, 2009, 21, 2755-2762.
9. Y. Yamazaki, F. Blanc, Y. Okuyama, L. Buannic, J. C. Lucio-Vega, C. P. Grey and S. M. Haile, *Nat Mater*, 2013, 12, 647-651.
10. P. L. Knochel, P. J. Keenan, C. Loho, C. Reitz, R. Witte, K. S. Knight, A. J. Wright, H. Hahn, P. R. Slater and O. Clemens, *J Mater Chem A*, 2016, 4, 3415-3430.
11. P. A. Sukkurji, A. Molinari, A. Benes, C. Loho, V. S. K. Chakravadhanula, S. K. Garlapati, R. Kruk and O. Clemens, *Journal of Physics D-Applied Physics*, 2017, 50.
12. A. Benes, A. Molinari, R. Witte, R. Kruk, J. Brotz, R. Chellali, H. Hahn and O. Clemens, *Materials (Basel)*, 2017, 11.
13. H. J. Hwang, M. B. Ji-Woong, L. A. Seunghun and E. A. Lee, *J Power Sources*, 2005, 145, 243-248.
14. Z. Shao and S. M. Haile, *Nature*, 2004, 431, 170-173.
15. E. Fabbri, R. Mohamed, P. Levecque, O. Conrad, R. Kötz and T. J. Schmidt, *ACS Catalysis*, 2014, 4, 1061-1070.
16. U. Spitsbergen, *Acta Crystallogr*, 1960, 13, 197-198.
17. K. Boulahya, M. Parras, J. M. Gonzalez-Calbet, U. Amador, J. L. Martinez, V. Tissen and M. T. Fernandez-Diaz, *Phys Rev B*, 2005, 71.
18. A. J. Jacobson and J. L. Hutchison, *J Chem Soc Chem Comm*, 1976, 116-117.
19. N. Raghu, V. Ravi and T. R. N. Kutty, *Materials Research Bulletin*, 1991, 26, 261-268.
20. Z. H. Hu, H. M. Zhang, J. H. Wang, L. Chen, X. X. Xie, X. Liu, J. C. Yao and A. M. Chang, *J Mater Sci-Mater El*, 2017, 28, 6239-6244.
21. P. M. Botta, V. Pardo, C. de la Calle, D. Baldomir, J. A. Alonso and J. Rivas, *J Magn Magn Mater*, 2007, 316, E670-E673.
22. J. L. Cacheiro, M. Iglesias, V. Pardo, D. Baldomir and J. E. Arias, *Int J Quantum Chem*, 2003, 91, 252-256.

View Article Online
DOI: 10.1039/C8DT01326H

23. T. Inoue, T. Matsui, N. Fujimura, H. Tsuda and K. Morii, *Ieee T Magn*, 2005, 41, 3496-3498.
24. R. Djenadic, M. Botros, C. Benel, O. Clemens, S. Indris, A. Choudhary, T. Bergfeldt and H. Hahn, *Solid State Ionics*, 2014, 263, 49-56.
25. *Topas V4.2, General profile and structure analysis software for powder diffraction data, User's Manual*, Bruker AXS, Karlsruhe, Germany, 2008.
26. R. W. Cheary, A. A. Coelho and J. P. Cline, *Journal of Research of the National Institute of Standards and Technology*, 2004, 109, 1-25.
27. D. Johnson, *Inc., Southern Pines, NC*, 2002, 200.
28. A. Sarkar, R. Djenadic, D. Wang, C. Hein, R. Kautenburger, O. Clemens and H. Hahn, *Journal of the European Ceramic Society*, 2018, 38, 2318-2327.
29. V. Jayaraman, A. Magrez, M. Caldes, O. Joubert, F. Taulelle, J. Rodriguezcarvajal, Y. Piffard and L. Brohan, *Solid State Ionics*, 2004, 170, 25-32.
30. I. D. Brown, *The chemical bond in inorganic chemistry: the bond valence model*, Oxford University Press Inc., New York, 2002.
31. R. Zohourian, R. Merkle and J. Maier, *Solid State Ionics*, 2017, 299, 64-69.
32. J. Bielecki, S. F. Parker, L. Mazzei, L. Borjesson and M. Karlsson, *J Mater Chem A*, 2016, 4, 1224-1232.
33. W. Fischer, G. Reck and T. Schober, *Solid State Ionics*, 1999, 116, 211-215.
34. L. Truong, M. Howard, O. Clemens, K. S. Knight, P. R. Slater and V. Thangadurai, *J Mater Chem A*, 2013, 1, 13469-13475.
35. V. E. H. Richard L. Kurtz, Roger Stockbauer, Theodore E. Madey, Donald Mueller, Arnold Shih, Louis Toth, *Phys Rev B*, 1988, 37, 7936-7939.
36. R. L. Kurtz and V. E. Henrich, *Phys Rev B*, 1982, 26, 6682-6689.